Gas Streams and Spiral Structure in the Milky Way

Peter Englmaier

Max-Planck-Institut für extraterrestrische Physik
Postfach 1603, D-85748 Garching, Germany
ppe@mpe.mpg.de

Abstract

The observed gas dynamics in the Milky Way can only be explained by a bar in the galactic center. Such a bar is directly visible in the near-IR maps of the bulge, where it causes a distinctive asymmetric light distribution pattern. Another large-scale structure is the grand-design 4-arm spiral pattern, most clearly observed in the spatial distribution of molecular gas and H II-regions. Since this spiral arm pattern is regular, it must have existed for at least a few rotations. Traced by molecular clouds, the spiral arms appear strongest in the so-called molecular ring between 4 and 7 kpc.

In order to model the observed gas flow structure, we constructed a model for the stellar mass distribution. For the inner 5 kpc *we used the 3D deprojected near-IR light distribution, as observed by the COBE/DIRBE experiment, and added an analytical disk model outside the box as well as a halo model. With this frozen mass distribution, we computed the stationary gas flow for various deprojection parameters and pattern speeds. For all reasonable parameter choices, we obtain a 4-armed spiral pattern, which can be matched to the observed spiral arms. The model spiral arms, are caused by the forcing of the bar, and two additional mass concentrations at about 4 kpc's on the minor axis of the bar, which are likely to be incorrectly deprojected stellar spiral arms.*

In the bar region, our model can explain the non-circular motion visible in the terminal velocity curve as well as some part of the forbidden velocities. Inside the corotation, we also find 4 spiral arms, the nearest arm corresponds to the 3-kpc-arm, although only qualitatively. The missing southern 3-kpc-arm at the far end of the galaxy is explained by running parallel to another arm. Close to the center, we find gas on circular orbits forming a disk. Such a disk has been observed in emission of the CS molecule, however only part of the disk appears to be occupied by dense enough gas to be traced by CS. Finally, we compare the observed distribution of OH/IR stars with predictions of our model.

1 Introduction

The Milky Way is our local laboratory of star formation and ISM physics. Some observations even have only been possible in the Milky Way, e. g. turbulent motion and magnetic field in ISM clouds, or search for dark matter candidates. Also, many observable quantities are directly linked to the history and structure of the Milky Way, e. g. metalicity gradients (Friedli 1999), and distribution of OH/IR stars (see below). A better understanding of the detailed mass distribution and gas flow will therefore benefit many other studies.

Morphology and type of the Milky Way are hard to recognize because of dust obscuration and the location of the sun within the disk. Spiral arm tangents can be identified in optical and radio brightness distributions (Sofue 1973), as well as in molecular gas (e. g., Dame *et al.* 1987), HII regions (Georgelin & Georgelin 1976), and other tracers; see Vallée (1995) for a complete list. The 3-kpc-arm, is unusual in this respect: it is very bright in CO, but not traced by HII regions. It is therefore possible that it does not form stars at the present time. Maybe this is because it has an enhanced turbulent velocity or a higher differential shear (Rohlfs & Kreitschmann 1987). The 3-kpc arm and other peculiar gas dynamics in the galactic center are evidence for a bar in the bulge region. The other spiral arms outside the bar region within the so-called molecular ring appear to be on almost circular orbits since they do not show large non-circular motion in front of the galactic center. A comparison of many publications indicates that the Milky Way most likely has 4 spiral arms with a pitch angle of 12° (Vallée 1995).

Another important aspect is, that the true rotation curve of the Milky Way can be measured more precisely by a combination of a stellar mass model and a hydrodynamical model. When the rotation curve is determined from the gas dynamics alone, an axisymmetric model yields an uncommon sharp peak at $\sim 0.5\,\mathrm{kpc}$ (Clemens 1985). An axisymmetric model of the stellar mass distribution, however, implies a mostly flat rotation curve there (Kent 1992). A bar naturally solves this issue by explaining the sharp peak with non-circular motion caused by orbits elongated along the bar (Binney *et al.* 1991). It also explains the observed nuclear disk of molecular gas inside $\sim 200\,\mathrm{pc}$.

Finally, having a better model for the mass distribution and rotation curve, one also obtains better constraints on the amount of dark matter in the solar neighborhood.

Since a short review cannot give a complete coverage of all Milky Way models in the literature, we refer the reader to the following papers for similar and alternative models: Lin, Yuan & Shu (1969), Mulder & Liem (1986), Amaral & Lépine (1997), Wada *et al.* (1994), Weiner & Sellwood (1999), and Fux (1999a). For reviews about spiral structure see: Wielen (1974), Toomre (1977), Binney & Tremaine (1987), and Bertin & Lin (1996).

2 Using observations to yield a detailed mass model

An early axisymmetric mass model for the inner Galaxy was constructed by Kent, Dame & Fazio (1991), by fitting parametric models to the photometric near-IR maps at 2.4 μm (K-Band) which where obtained by the Spacelab Infrared Telescope (IRT) and have a resolution of 1°. By assuming a constant mass-to-light ratio for each component Kent (1992) found various possible combinations of bulge, disk, and halo components to fit the observed mass distribution and kinematics, as well as the gaseous rotation curve outside the bulge region. The bulge region was excluded from the fit, because the gaseous rotation curve from Clemens (1985) shows signs of non-circular motion due to the presence of a bar. Since the dark halo is only observable through its gravitational interaction, Kent used the dark halo component to compensate for the mismatch between gaseous rotation curve and the rotation curve implied by the disk and the mass distribution in the inner galaxy. He also defined a maximum disk model, which minimizes the amount of dark matter required by maximizing the mass-to-light ratio for the disk (he found $M/L = 1.3$). This model is particular interesting, because it gives a lower limit for the amount of dark matter in the solar neighborhood. One reason why there is large uncertainty about the relative contribution of dark halo and disk, is that not enough constraints about the vertical distribution of mass in the galaxy are known (Dehnen & Binney 1998).

A major improvement over the model of Kent was made possible by the near-IR maps obtained with the DIRBE experiment on board of the COBE satellite. By using a foreground dust screen model, Dwek *et al.* (1995) found, that the bulge light is best fitted by a triaxial light distribution. This bar appears to be elongated with axis ratios $1 : 0.33 : 0.22$, the nearer end at positive longitudes and inclined by about 20°. Later, an improved dust correction and improved parametric model was obtained by Freudenreich (1998).

Another line of models comes from a non-parametric deprojection method introduced by Binney & Gerhard (1996). No parametric model distribution has to be prescribed, but an initial model has to be given. The method can also be applied to a part of the galaxy, while the model outside that part stays fixed as specified by the initial parametric model. Binney, Gerhard, & Spergel (1997) applied the method to the DIRBE data and found, that the result is robust against changes in the initial model and can reliably recover the 3D light distribution in the bulge. They also found additional light concentrations on the minor axis of the bar, which they attribute to spiral arm heads in that area. While the deprojection method is not able to recover spiral arm structure, tests show that spiral arms could produce clumps on the minor axis like the ones found in the DIRBE data. The only free parameters in this model are the mass-to-light ratio and the orientation of the bar. See Gerhard (1996, 1999) for a comparison of these models and further evidence for the bar.

For further modeling, we expanded the mass model from Binney, Gerhard, & Spergel (1997) into a series of spherical harmonics to calculate the gravitational potential. The radial density profile in the galactic center follows a power law $\rho \propto r^{-1.85}$ (Becklin & Neugebauer 1968) and this peak in the density is not reproduced by the deprojection because of finite resolution and smoothing effects. We therefore corrected the zeroth order spherical harmonic (monopole) to reflect the power law.

The resulting rotation curve falls off beyond 4.5 kpc, because no dark halo has been included yet. By construction, the model should reflect the contribution of all luminous mass in the galaxy without any assumptions about how bulge and disk are build together assuming the same M/L. For some models, we changed the monopole to allow for a flat rotation curve.

3 Terminal rotation curve

The rotation curve of the Milky Way is not directly observable. In external galaxies, the rotation curve can be obtained by an observation of Doppler shift along a slit across the center. Using parametric models for disk, bulge and halo, the rotation curve can then be decomposed. The parametric model for disk and bulge must follow the observed surface brightness, while the dark matter halo is only constrained by the fit to the rotation curve. Where density wave theory is applicable, i. e. for tightly wound spirals, further constraints are available for the dark matter contribution (Fuchs, Möllenhoff & Heidt 1998).

In the Milky Way, the rotation curve can only be inferred indirectly from the terminal velocity, i.e. the maximum observed radial velocity within the galactic plane at a given longitude. Historically, the terminal rotation curve, has been used to infer the radial mass distribution by assuming circular rotation. Inside the solar circle, the terminal velocity is equal to the circular rotation curve minus the motion of the local standard of rest (LSR). The motion of the LSR can be inferred from the streaming of stars measured by Hipparcos (Feast & Whitelook 1997), or the proper motion of Sgr A* (Backer & Stramek 1999). Both methods agree reasonable well, and no $m = 1$ mode seems to be present in the center of the galaxy.

The high peak in the terminal curve, gas on apparently forbidden velocities, and the large radial velocity of the 3-kpc-arm indicate non-circular motion in the inner galaxy. This led to the idea, that our galaxy is actually barred and the presence of a bar implies non-circular motion which cannot be corrected for without modeling (Gerhard & Vietri 1986). Fortunately, the non-axisymmetric light distribution of the bar can be extracted from photometric imaging due to perspective effects. These effects are only strong enough if the diameter of the stellar system is comparable to its distance. This excludes application of similar models for distant objects in the near future. A non-parametric method for the deprojection has been recently developed by Binney & Gerhard (1996). Its main advantage over parametric

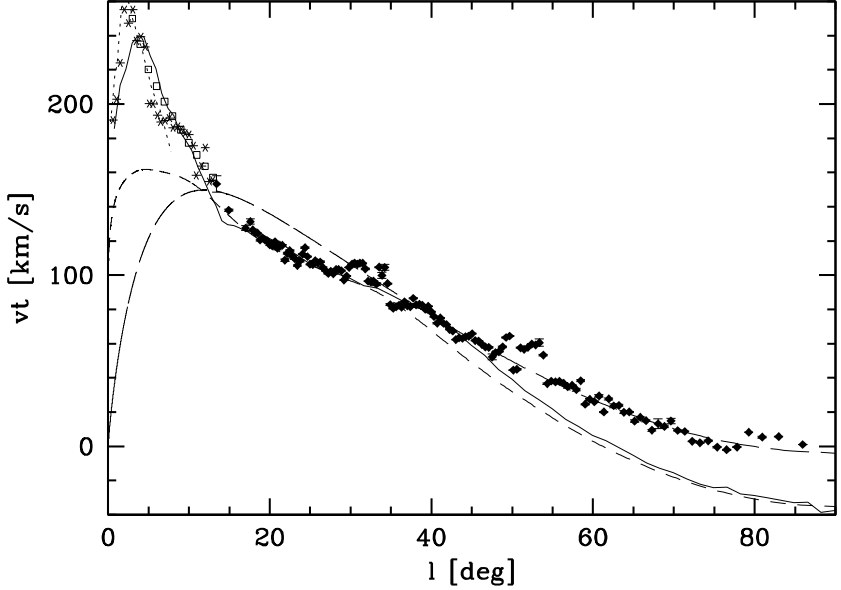

Figure 1: Terminal curve for Kent (1992, long-dashed line), axisymmetric BGS model without halo (short dashed line), and gas dynamics in full BGS model without halo (solid line and dotted line with higher resolution).

methods is, that it allows to recover more structure details and the precise radial mass distribution. But an application of this method to the DIRBE data yielded controversial results (Binney, Gerhard & Spergel 1997; in the following: BGS). The recovered radial and vertical structure of bar and disk provides a realistic view of the inner galaxy. But in addition, mass concentrations on the minor axis have been found in the deprojection, which seem to indicate that the inner galaxy has significant spiral structure as well.

In Fig. 1 we compare the axisymmetric part of the BGS model (short dashed line) with the axisymmetric model by Kent (1992, long dashed line) and the ^{12}CO data from Clemens (1985) and H I data from Burton & Liszt (1993). Note that Kents model includes a dark halo and assumes LSR motion $V_0 = 234\,\mathrm{km\,s^{-1}}$ while the BGS model was plotted for $V_0 = 220\,\mathrm{km\,s^{-1}}$ and does not include a halo. Increasing the LSR motion increases the gap between model and observed terminal curve at the solar circle ($l = 90°$), but can be compensated for with a dark matter component.

Both axisymmetric models fail to explain the peak in the rotation curve. Between 15 and 40° the BGS model fits the data better, further out the contribution of the dark halo is missing which is already included in Kents model. When we assume a constant rotation curve beyond 5 kpc (= 40°), the BGS model also matches the data between 40° and 90°. Closed orbits in the full BGS potential match the high peak in the rotation curve (Fig. 2). This confirms that the deprojection indeed provides a good description of the bar

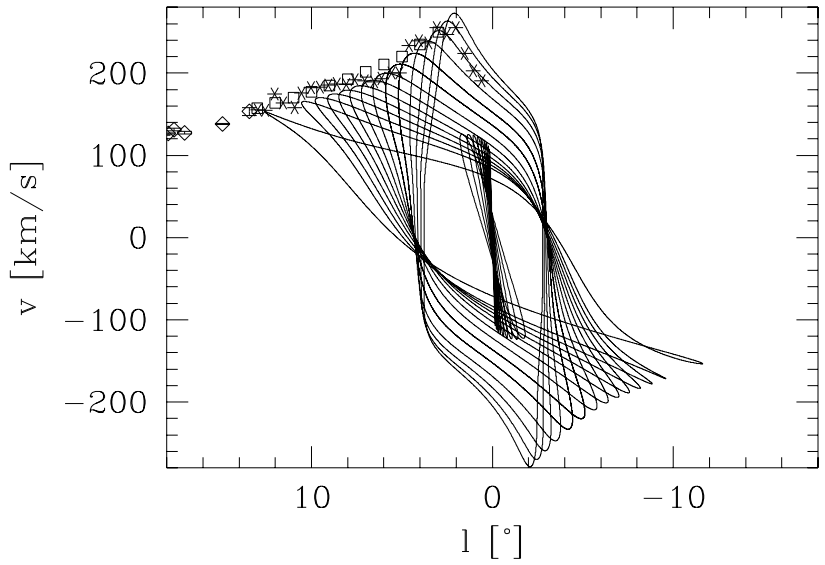

Figure 2: The high peak in the observed terminal velocity curve (points) is reproduced by the x_1-orbital family in the BGS model.

potential. Further out, the combination of bar and mass concentration on the minor axis complicates the picture. A hydrodynamical model of the gas flow in the BGS model is presented below. When the terminal curve for this model is compared to the data (Fig. 1; solid line), the result depends on the resolution in the gas model. Hydrodynamical forces tend to depopulate the orbits responsible for the peak in the rotation curve due to low resolution. A model with higher resolution matches the peak better (Fig. 1; dotted line).

Whether bars and spirals are independent dynamical entities is not yet clear and may vary from galaxy to galaxy. Numerical N-body simulations show that a bar can coexist with a spiral of much lower pattern speed (Sellwood & Sparke 1988). On the other hand, detailed modelling of the observed gas dynamics in NGC 1365 was possible using bar and spiral perturbation with a single pattern speed (Lindblad, Lindblad & Athanassoula 1996).

Moreover, the spiral mode is most likely growing and decaying within a few rotations of the galaxy (Lin & Shu 1964). For our gas model, we assumed that these additional light concentrations can be used as a first approximation to the contribution of spiral arms in this region and that the spiral pattern is rotating with the same speed as the bar and is stationary.

A more advanced deprojection technique combined with spiral arm modeling will be used to shed more light on this issue shortly (Bissantz & Gerhard 2000). This will also allow us to study models with independently rotating bar and spiral mode.

4 Steady state / Stationary gas flow solution

If the gas is allowed to relax in the potential of the galaxy, i. e. the mass distribution in the galaxy does not change over a few rotational periods, we expect the gas to form a stationary flow pattern. Since the gas looses energy in collisions, it arranges itself to follow nested closed orbits which have no intersections. In barred galaxies, orbits are organized in families. The so-called x_1-orbits are elongated along the bar and exist from somewhat inside the corotation annulus to the center. Inside the bar region there is a special cusped x_1-orbit, which is the last x_1 orbit the gas can settle on. Inside this orbit, the x_1 orbits in our potential develop loops with self-intersections. Gas on such orbits, would suffer collisions causing it to leave the orbit. In linear theory, the gas has to pass through the inner Lindblad resonance (ILR), which causes a phase shift of $\pi/2$ in the orbits. The gas follows this phase shift with a delayed response, and switches to the x_2 family of orbits, which are elongated perpendicular to the bar and exist only inside the ILR. In general, further ILRs may exist, but there is no evidence for further ILRs in the BGS potential. The transition at the ILR is not smoothly, but is accompanied by a shock in the gas flow. In strong bars, the shocks are straight lines, which in real galaxies have been identified with dust lanes and velocity jumps. Due to the non-axisymmetric distribution of gas caused by the shocks or spiral arms, the bar imposes a gravitational torque on the gas, which causes the gas to flow in (out) when the trailing spiral arm is inside (outside) corotation. For leading spiral arms, the torque would be reversed. For this reason, gas is slowly depleted in the corotation region and accumulates within the ILR to form a ring or disk of gas on x_2 orbits.

For hydrodynamics we chose the smooth particle hydrodynamics (SPH) method (Benz 1990; Steinmetz & Müller 1993). In SPH a continuous gas distribution is approximated by a spatially smeared out particle distribution. The advantage of this method is, that self-gravity can easily be included. Further numerical details of this simulation are given in Englmaier & Gerhard (1999). In addition to the free parameters from the deprojection, our gas model needs only three additional parameters: the corotation radius or equivalently the pattern speed, the effective sound speed, and the LSR motion for calculation of (lv) diagrams. Our best model is shown in Fig. 3.

The corotation radius in our model is tightly constrained by the observed (lv)-diagram as follows. Since the 3-kpc-arm is clearly in non-circular rotation, it must be inside the corotation radius. By comparison, the 4-armed spiral pattern in the molecular ring between 4 and 7 kpc shows no large deviation from circular motion. This observation can only be reproduced in our model, if the corotation is between 3 and 4 kpc. The angular extend of the 3-kpc-arm is best reproduced for corotation at 3.4 kpc.

The M/L ratio and the LSR motion are fixed by a fit of the terminal velocity curve to the model. Actually the circular rotation velocity for the LSR is kept constant to $200\,\mathrm{km\,s^{-1}}$ times a scaling constant which depends on M/L. The final value for the LSR motion is $208\,\mathrm{km\,s^{-1}}$ after the best

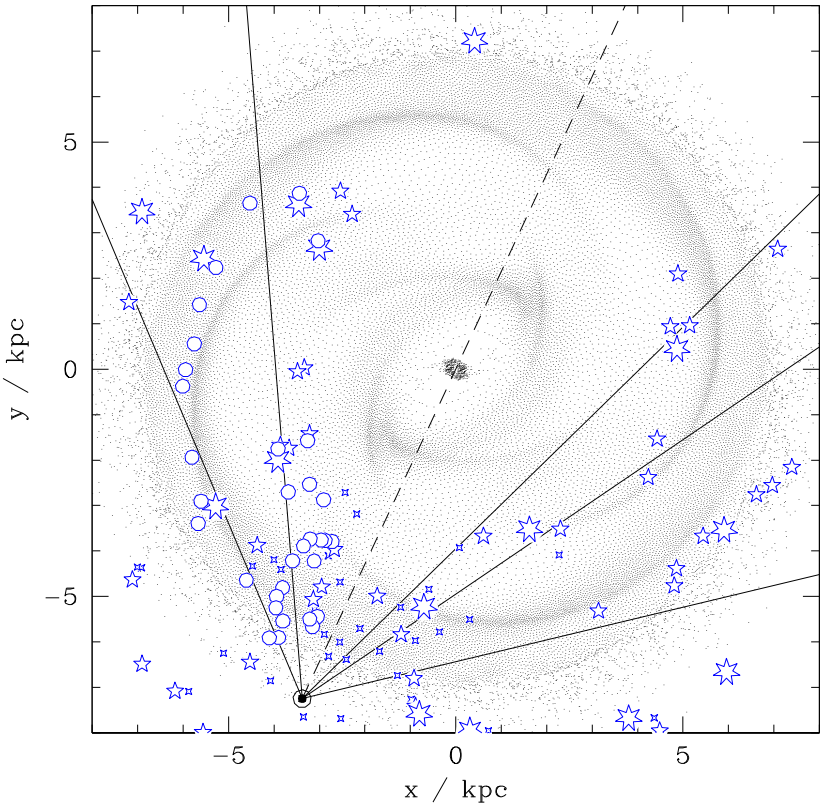

Figure 3: Comparison of our model with observed spiral arm tangents (lines, averaged values) and H II regions (stars) and giant molecular clouds from Dame *et al.* (1986; circles). Rotation is clock wise, and the model is viewed from the north galactic pole. The bar inclination is 20° and corotation at 3.4 kpc. This model also includes a dark halo.

model fit has been determined. While this value is lower than the current best estimate for the LSR motion, we note that the M/L value and other model details do not depend strongly on this parameter. The difference in the terminal curve can be compensated for by a dark halo.

The gas flow model confirms the allowed range for the bar inclination found by BGS (25 ± 10). Models with 20° or 25° yield a better overall fits than models with 15° or 30°. A better model for the stellar spiral arms may improve this situation.

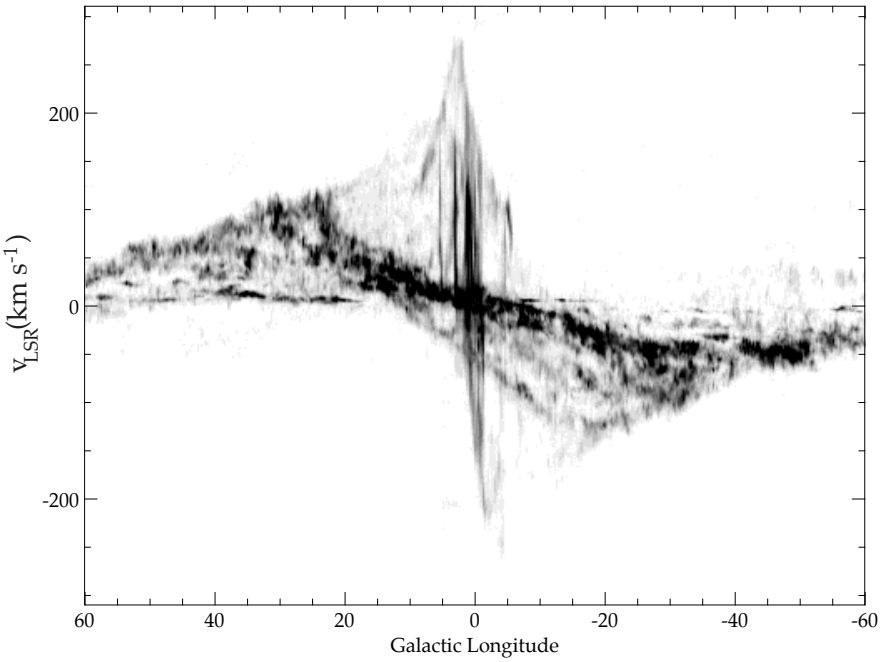

Figure 4: The (lv)-diagram for ^{12}CO from unpublished data by Dame *et al.* (1998). This figure contains all emission integrated over latitudes between $b = -2^\circ$ and $b = 2^\circ$. The grey scale is adjusted such as to emphasize spiral arm structures.

5 Identification of spiral arms in the (lv)-diagram

A full sky survey of emission from atomic hydrogen and molecular species like ^{12}CO allow mapping of large scale structure such as spiral arms (Fig. 4). The longitude-velocity diagram (lv-diagram) shows traces of spiral arms as crowded regions. By assuming circular rotation, one could map the observed (lv)-position back to real space, however, this leads to serious errors close to tangential points (Burton 1971). Nevertheless, with some success, the principle spiral arm structure has been inferred from lv-diagrams. First, this was done by Oort, Kerr & Westerhout (1958), later the 4-armed structure was first claimed by Georgelin & Georgelin (1976) using the (lv)-diagram for large HII-regions. This picture has later been refined by Caswell & Haynes (1987), Lockman (1989), and others. In Fig. 3 we compare various known HII-regions and giant molecular clouds from the literature with our model.

HII-regions are a particular good tracer for spiral arms, as is known from observations of external galaxies. The 4 spiral arms are also prominent in the so-called molecular ring between 4 and 7 kpc. This area corresponds to a bright band of ^{12}CO emission between about $30 \ldots 60^\circ$ on the northern side of the galaxy (left in Fig. 4) to $-(30 \ldots 60)^\circ$ on the southern side. As Solomon *et al.* (1987) pointed out, the spiral arm tangent at around $+30^\circ$ is actually

Indicator	Scutum far 3-kpc	Aquilla	Centaurus	Norma	3-kpc
(1)	29	50	-50	-32	
(2)	24, 30.5	49.5	-50	-30	
(3)	25, 32	51			
(4)	25, 30	49			
(5)	24, 30	47	-55	-28	
(6)	32	46	-50	-35	
(7)	32	48	-50,-58	-32	-21
(8)	29			-28	-21
(9)	26		-47	-31	-20
average	**30**	**49**	**-51**	**-31**	**-21**
Model					
(a)	~ 25	54	-44	-33	-20
(b)	~ 30	50	-46	-33	-20
(c)	~ 29	51	-47	-34	-22

Table 1: Measured spiral arm tangents in inner galaxy: (1) atomic hydrogen (Weaver 1970; Burton & Shane 1970; Henderson 1977); (2) integrated ^{12}CO (Cohen *et al.* 1980; Grabelsky *et al.* 1987); (3) ^{12}CO clouds (Dame *et al.* 1986); (4) warm CO clouds (Solomon *et al.* 1985); (5) H II-Regions using H109-α (Lockman 1979; Downes *et al.* 1980); (6) ^{26}Al from massive stars (Chen *et al.* 1996); (7) Radio 408 MHz (Beuermann *et al.* 1985); (8) 2.4 μm (Hayakawa *et al.* 1981); (9) 60 μm (Bloemen *et al.* 1990). Compared to some models: (a) $R_c = 3.4$ kpc, bar inclination $\varphi = 20°$, without halo; (b) $R_c = 3.4$ kpc, $\varphi = 20°$, with halo $v_0 = 200\,\mathrm{km\,s^{-1}}$; (c) $R_c = 3.4$ kpc, $\varphi = 25°$, with halo $v_0 = 200\,\mathrm{km\,s^{-1}}$.

split into two components at 25° and 30°. A summary of available spiral arm tangent data is listed in Table 1.

The molecular emission also shows an arm apparently not traced by H II-regions: the 3-kpc-arm. This arm shows large non-circular motion, as it passes in front of the galactic center (where it appears in absorption) with $+54\,\mathrm{km\,s^{-1}}$ radial velocity. All other arms show much less radial velocity in front of the galactic center.

Our gas model qualitatively reproduces many of the prominent features in the observed (lv)-diagram (Fig. 4). The four spiral arms are found to be embedded in the molecular ring with about the right tangential directions (see Table 1). Our model, however, assumes perfect point symmetry in the gas, while the galaxy is not. Hence a perfect match cannot be expected in such an idealized model. Inside the molecular ring, gas is depleted in the corotation region and the spiral arms show a gap (see Fig. 3). Within corotation the spiral pattern continues followed by the usual gas flow configuration in a barred galaxy (see previous section). One of the spiral arms is similar to the 3-kpc-arm in the galaxy, alas with too small an expansion velocity. In

this region, the gas flow may be disturbed by the stellar spiral arms. In a modified model where we approximate the spiral arm gravity by the gaseous model spiral arms, but spatially smeared out to account for wider stellar spiral arms, the 3-kpc-arm can be reproduced quantitatively (Englmaier & Gerhard 1999). Our model also predicts the location of the arm corresponding to the 3-kpc-arm on the far side of the galaxy. It happens to fall close to the molecular ring and indeed this arm tangent was found to be split into two components by Solomon *et al.* (1987) and is also visible at $l = 25°, 30°$ in Fig. 4. A similar position for the far 3-kpc-arm was suggested by Sevenster (1999), but see Fux (1999a) for an alternative explanation. A nuclear disk with $\sim 200\,\mathrm{pc}$ radius is formed in the model by gas on x_2-orbits. Size and rotational velocity of this disk depends on the enclosed mass which has been adjusted by the central density cusp profile. While the disk matches the observed CS emission (Stark *et al.* 1991), only part of the disk is occupied by dense enough gas to show CS emission.

6 OH/IR stars as a fossil dynamical record

Sevenster (1997, 1999) made a complete sample of the OH/IR stars in the bulge region between $-45° \leq l \leq 10°$ and $|b| \leq 3°$. The OH/IR stars are giant stars that lose matter in the so-called asymptotic giant branch (AGB) superwind phase. While these stars are quite old, i. e. $\sim$ 1 to 8 Gyr, they quickly go through an evolutionary phase characterized by OH maser emission in the IR. The maser emission lasts only for $\sim 10^{5-6}\,\mathrm{yr}$ which is short compared to dynamical timescales. The sample of OH/IR therefore provides a snapshot of the dynamically evolved star formation regions $\sim$ 1 to 8 Gyr ago. Sevenster (1999) found, that the lv-diagram for the sample shows a striking correlation between the OH/IR stars and the 3-kpc-arm observed in ^{12}CO. A young group of about 100 to 350 Myr old OH/IR stars follows this arm very nicely, while the older OH/IR population is more equally distributed. This appears to be in contradiction with dynamics, since a circular orbit at 3 kpc takes $\sim 2\pi r/v \sim 80\,\mathrm{Myr}$ to complete. Any trace of the spatial distribution of star formation would have been wiped out. However, if these stars were formed in one of the spiral arms which itself rotates, then only the relative orbit between stars and arm would matter. For a constant pattern speed equal to the bar pattern speed, say $\Omega \sim 60\,\mathrm{km\,s^{-1}\,kpc^{-1}}$, the orbit in the rotating frame of the arm would take about $\sim 2\pi r/(v - \Omega r) \sim 0.5\,\mathrm{Gyr}$ to complete. This much longer timescale may allow stars formed at the same place to generate a distribution similar to the observed one. Furthermore, the 3-kpc-arm is not a strong shock, making it possible for stars formed within to drift away rather slowly.

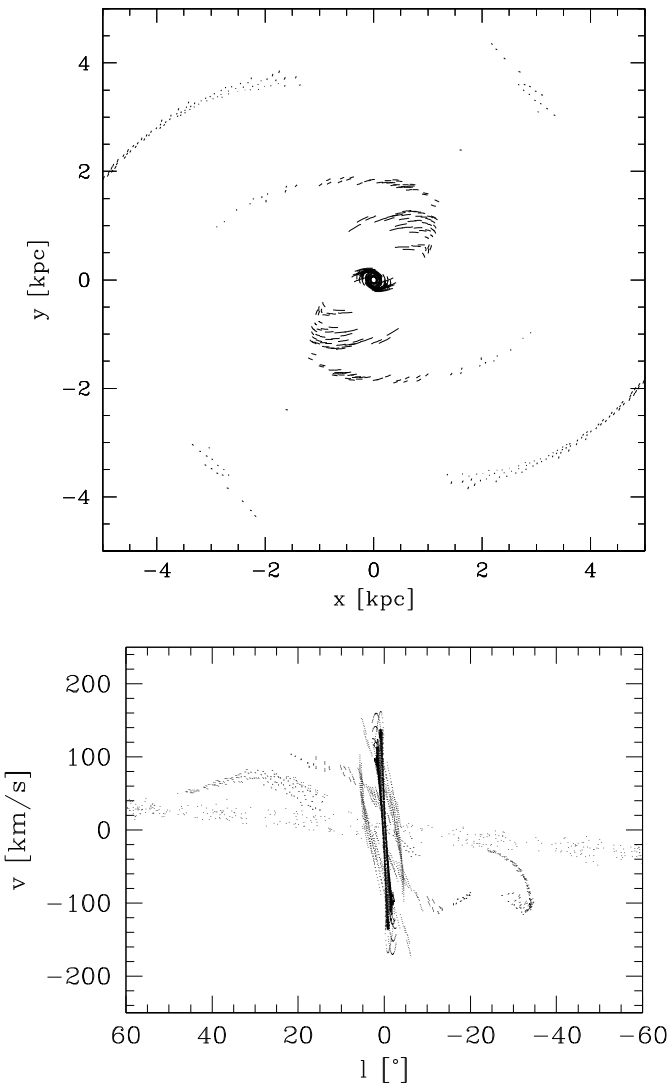

Figure 5: Location of star forming regions of compressed gas in face-on view (upper) and seen in the (lv)-diagram (lower). For each particle a 2 Myr long trace of its orbit is shown, which is approximately the duration of the OH/IR phase. The bar is aligned with the diagonal line from the lower left to the upper right (compare with figure 3). The sun to galactic center line is inclined 25° to the bar. The location of the sun is just outside the diagram at $x \approx -2.7\,\mathrm{kpc}$, $y \approx -7.5\,\mathrm{kpc}$. The 3-kpc-arm is the horizontal trace of stars starting at the lower left end of the bar. For the (lv)-diagram a circular velocity of $220\,\mathrm{km\,s^{-1}}$ has been used for the transformation in the LSR. The 3-kpc-arm passes the galactic center ($l = 0°$) with the velocity $\sim -40\,\mathrm{km\,s^{-1}}$ and continues to $l = -21°$, $v = -100\,\mathrm{km\,s^{-1}}$.

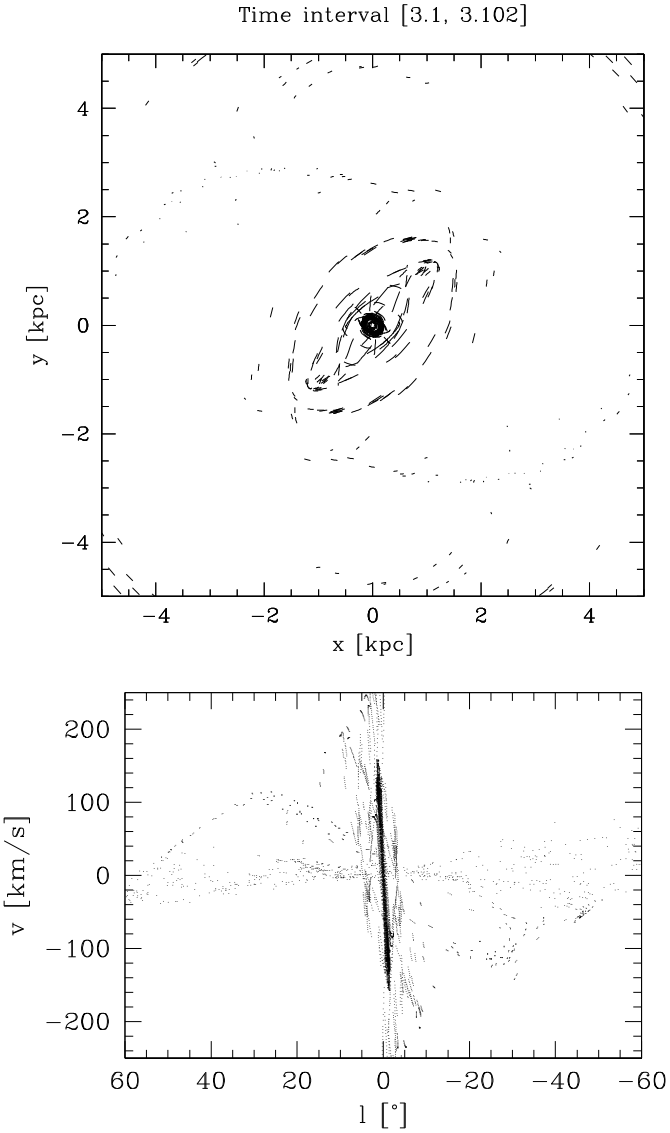

Figure 6: Same as figure 5, but 100 Myr later. Stars created in the 3-kpc-arm have formed elliptical rings aligned with the bar which do not follow the 3-kpc-arm in the (lv)-diagram, but are restricted to $|l| < 10°$. However, a trace of stars originally created in the corotation region forms a bridge between corotation and ends of the bar maintaining a 3-kpc-arm alike structure in the (lv)-diagram.

In order to estimate the dynamical constraints of our model on the observed OH/IR star distribution, we picked our best model and selected gas particles which are in compressed areas, i. e. in spiral arm shocks (see Fig. 5). We evolved these particles as test particles in the background potential of the model, and plotted snapshots for the particle distribution at later times. It turns out that, although OH/IR stars may form a transient arm like feature, it will only last for a few 100 Myr. In Fig. 6, we show the lv-diagram for 100 Myr old stars. There is a 3-kpc-arm-like distribution of stars, but these stars come from the corotation region at the minor axis, not the 3-kpc-arm. Just inside corotation, a star formed from the gas moves faster than the bar pattern, and this gives raise to a coriolis force pulling the star inwards. A group of freshly formed but isolated stars would form a stream which may be coincident with the 3-kpc-arm. As we discussed above, the 3-kpc-arm does not contain H II-regions and presumably, it does not form stars because it is dynamically hot. Stars which are formed in the 3-kpc-arm are quickly distributed on closed orbits, it is therefore possible that OH/IR stars are indeed distributed in rings indicating radii of more compressed gas in our model, and these orbits, which are not circular orbits, may be indirectly correlated with the 3-kpc-arm, because arms which are driven by a bar, often start with a local density enhancement and strong star formation on the bar major axis. However, we would expect those rings to be inclined with respect to the 3-kpc-arm, unless the 3-kpc-arm is not stationary.

A similar result was found by Fux (1999b), where the observed OH/IR star distribution could be reproduced for about 40 Myr old stars. The OH/IR stars in his model originate in the far end of the bar in an area of enhanced density. Contrary to our model, Fux's model has the additional advantage, that the 3-kpc-arm changes rapidly and thus the gas is on more ballistic orbits. He did not show any evidence, however, that the coincidence of stars and gas can be maintained over multiple rotations as required by the observations. While both models are optimized to fit various aspects of the Milky Way, they both suggest that OH/IR stars are not directly tracing spiral arms.

We therefore consider it more likely that the stars formed close to corotation where timescales are comparable to the age of these stars. It will be interesting if further evidence can be found, to show that OH/IR stars follow closed orbits and whether these favored orbits have changed with time.

7 Discussion

We presented a coherent description for the structure and gas dynamics in the Milky Way reaching from small scale ~ 100 pc to large scale $\sim$ kpc. Our model provides a link between photometric and gas dynamical observations, but does not intend to be a a self-consistent treatment of formation and evolution of the Milky Way. Idealized assumptions about symmetry and in the description of the ISM have been made to isolate generic from peculiar features.

We find, that the 3-kpc-arm can be explained qualitatively by the forcing of the bar. The bar may also be responsible for some of the spiral structure observed in the gas. Strong bars can drive spiral arms to and somewhat beyond the outer Lindblad resonance (Mulder 1986). The deprojection of the near-IR bulge light distribution introduced additional structure on the minor axis of the bar at around corotation. When this structure is included into the model, four spiral arms are driven in the gas similar to the observed spiral arm structure in this region. The pattern is very similar to a model by Mulder & Liem (1986), but the location of the sun is different. Interestingly, Mulder (1986) mentions that this pattern can be driven by a strong bar or by a weak bar plus spiral arms beyond corotation.

When the gravity of the spiral arms is included in the model, the 3-kpc-arm can also be explained quantitatively. This finding, and in addition our inability to find a fitting model for the 3-kpc-arm in models without the minor axis structure demonstrates, that the inner galaxy is affected by both bar and spiral arms.

While spiral arms in barred galaxies usually start at the end of the bar, they do not need to be driven by the bar (Sellwood & Sparke 1988), and might be dynamically independent with much lower pattern speed. No steady state but maybe a periodic steady state can be found in the gas flow of such a model. Independent stellar spiral arms further complicate the gas dynamics to some extent, because they cause non-linear velocity jumps in the gas and will not just add to the structure formed by the bar. From density wave theory (Lin & Shu 1964) we know, that spiral arms are not stationary but form and decay in a few rotational periods. With a lower pattern speed, the spiral pattern would extend to larger radii. A model for the galaxy, where spiral arms and bar have different pattern speeds has still to be constructed, yet.

Considering all these objections, it is even more surprising how well our model explains the spiral structure. Both the bar and the spiral pattern impose similar constraints on the orientation of the pattern, i.e. the phase angle. Nevertheless, this overlap might be a mere coincidence and a better treatment of bar and spiral mode is underway to investigate other possibilities (Bissantz *et al.*, in prep.).

Acknowledgements

I want to thank O. Gerhard for his collaboration on this project. This work was supported by the Swiss NSF grants 21-40'464.94 and 20-43'218.95.

References

Amaral L.H., Lépine J.R.D., 1997, MNRAS, 286, 885

Backer D.C., Stramek R.A., 1999, ApJ, 524, 805

Becklin E.E., Neugebauer G., 1968, ApJ, 151, 145

Benz W., 1990, in *The Numerical Modelling of Nonlinear Stellar Pulsations*, ed. Buchler J.R., p. 269, Dordrecht, Kluwer

Bertin G., Lin C.C., 1996, MIT Press, Cambridge, Mass.

Beuermann K., Kanbach G., Berkhuijsen E.M., 1985, A&A, 153, 17

Binney J.J., Gerhard O.E., Stark A.A., Bally J., Uchida K.I., 1991, MNRAS, 252, 210

Binney J.J., Gerhard O.E., 1996, MNRAS, 279, 1005

Binney J.J., Gerhard O.E., Spergel D.N., 1997, MNRAS, 288, 365

Binney J.J., Tremaine S., 1987, Princeton University Press

Bissantz N., Gerhard O.E., 2000, in prep.

Bloemen J.B.G.M., Deul E.R., Thaddeus P., 1990, A&A, 233, 437

Burton W.B., 1971, A&A, 10, 76

Burton W.B., Shane W.W., 1970, IAU Symposium 38, eds. Becker W., Contopoulos G., Reidel, Dordrecht, p. 397

Burton W.B., Liszt H.S., 1993, A&A, 274, 765

Chen W., Gehrels N., Diehl R., Hartmann D., 1996, A&AS, 120, 315

Clemens D.P., 1985, ApJ, 295, 422

Caswell J.L., Haynes, R.F., 1987, A&A, 171, 261

Cohen R.J., Cong H., Dame T.M., Thaddeus P., 1980, ApJ, 239, L53

Dame T.M., Elmegreen B.G., Cohen R.S., Thaddeus P., 1986, ApJ, 305, 892

Dame T., *et al.*, 1987, ApJ, 322, 706

Dehnen W., Binney J.J., 1998, MNRAS, 294, 429

Downes D., Wilson T.L., Bieging J., Wink J., 1980, A&AS, 40, 379

Dwek E., *et al*, 1995, ApJ, 445, 716

Englmaier P., Gerhard O.E., 1999, MNRAS, 304, 512

Feast M., Whitelook P., 1997, MNRAS, 291, 683

Freudenreich H.T., 1998, ApJ, 492, 495

Friedli D., 1999, in *The Evolution of Galaxies on Cosmological Timescales*, eds. Beckman J.E., Mahoney T., ASP Conf. Series, astro-ph/9903143

Fuchs B., Möllenhof C., Heidt J., 1998, A&A, 336, 878

Fux R., 1999a, A&A, 347, 77

Fux R., 1999b, in *The Evolution of Galaxies on Cosmological Timescales*, eds. Beckman J.E., Mahoney T., ASP Conf. Series, astro-ph/9908091

Georgelin Y.M., Georgelin Y.P., 1976, A&A, 49, 57

Gerhard O.E., 1996, in: *Unsolved Problems of the Milky Way*, IAU Symp. 169, eds. Blitz L., Teuben P., p. 79

Gerhard O.E., 1999, in *Galaxy Dynamics*, eds. Merritt D.R., Valluri M., Sellwood J.A., ASP Conf. Series, p. 307

Gerhard O.E., Vietri M., 1986, MNRAS, 223, 377

Grabelsky D.A., Cohen R.S., Bronfman L., Thaddeus P., 1987, ApJ, 315, 122

Hayakawa S. *et al*, 1981, A&A, 100, 116

Henderson A.P., 1977, A&A, 58, 189

Kent S.M., 1992, ApJ, 387, 181

Kent S.M., Dame T.M., Fazio G., 1991, ApJ, 378, 131

Lin C.C., Shu F.H., 1964, ApJ, 140, 646

Lin C.C., Yuan C., Shu F.H., 1969, ApJ, 155, 721

Lindblad P.A.B., Lindblad P.O., Athanassoula E., 1996, A&A, 313, 65

Lockman F.J., 1979, ApJ, 232, 761

Lockman F.J., 1989, ApJ Suppl., 71, 469

Mulder W.A., 1986, A&A, 156, 354

Mulder W.A., Liem B.T., 1986, A&A, 157, 148

Oort J.H., Kerr F.T., Westerhout G., 1958, MNRAS, 118, 379

Rohlfs K., Kreitschmann J., 1987, A&A, 178, 95

Schmidt M., 1965, Bull. Astr. Inst. Netherlands, 13, 15

Sevenster M., 1997, thesis, Leiden

Sevenster M., 1999, MNRAS, in press, astro-ph/9907319

Sellwood J.A., Sparke L.S., 1988, MNRAS, 231, 25

Sofue, 1973, PASJ, 25, 207

Solomon P.M., Sanders D.B., Rivolo A.R., 1985, ApJ, 292, 19

Solomon P.M., Rivolo A.R., Barrett J., Yahil A., 1987, ApJ, 319, 730

Stark A.A., Bally J., Gerhard O.E., Binney J.J., 1991, MNRAS, 248, 14

Steinmetz M., Müller E., 1993, A&A, 268, 391

Toomre A., 1977, ARA&A, 15, 437

Vallée J.P., 1995, ApJ, 454, 119

Wada K., Taniguchi Y., Habe A., Hasegawa T., 1994, ApJ, 437L, 123

Weaver 1970, in: *The Spiral Structure of Our Galaxy*, IAU Symp. 38, eds. Becker W., Contopoulos G., Reidel, Dordrecht, p. 126

Weiner B.J., Sellwood J.A., 1999, ApJ, 524, 112

Wielen R., 1974, PASP, 86, 341